Structural insights into blue-green light utilization by marine green algal light harvesting complex II at 2.78 Å

Structural insights into blue-green light utilization by marine green algal light harvesting complex II at 2.78 Å

Soichiro Seki, Tetsuko Nakaniwa, Pablo Castro-Hartmann, Kasim Sader, Akihiro Kawamoto, Hideaki Tanaka, Pu Qian, Genji Kurisu, Ritsuko Fujii

Citation	BBA Advances. 2; 100064
Version of Record	2022-11-05
Type	Journal Article
Textversion	Publisher
Highlights	◇海洋性緑藻ミルの光合成アンテナの構造をクライオ電子顕微鏡法を用いて高分解能で解析 ◇光合成アンテナに結合している色素の構造と置換位置を解明
概要	研究グループは、高分解能の電子顕微鏡を用いた解析により、海洋性緑藻ミルの光合成アンテナと呼ばれるタンパク質内での色素の構造と結合環境を初めて明らかにしました。その結果、海水中で得られる唯一の光である青緑色光を効率よく光合成に利用する分子メカニズムがより鮮明になりました。
Supplementary materials	Supplementary material associated with this article can be found, in the online version: https://doi.org/10.1016/j.bbadva.2022.100064.
Rights	© 2022 The Author(s). Published by Elsevier B.V. This is an open access article under the CC BY license (https://creativecommons.org/licenses/by/4.0/).
DOI	10.1016/j.bbadva.2022.100064

Seki, S., Nakaniwa, T., Castro-Hartmann, P., Sader, K., Kawamoto, A., Tanaka, H., Qian, P., Kurisu, G., & Fujii, R. (2022). Structural insights into blue-green light utilization by marine green algal light harvesting complex II at 2.78 Å. *BBA Advances*. 2, 100064.
https://doi.org/10.1016/j.bbadva.2022.100064

Description	<研究の背景> 陸上に生息する植物は、太陽光の内、赤色と青色を主に吸収して光合成に利用します。しかし、海底には青緑色の弱い光しか届かないため、海洋に生育する大型藻はこの青緑色光を効率よく利用する光合成アンテナを発達させてきました。これは陸上植物の光合成アンテナと非常に似ていますが、結合している色素の構造に特徴があります。光合成アンテナというタンパク質にはカロテノイド色素とクロロフィル色素の二種類の色素が結合していますが、本研究対象の海洋性大型緑藻ミル（学名 Codium fragile, 図 1 上）では、カロテノイド色素がシフォナキサンチン(図 1 下)に、またクロロフィル色素の一部がクロロフィル *a* からクロロフィル *b* に入れ替わっています。前者は緑色光、後者は青緑色光の吸収量を増やすのに貢献していることが分かっていましたが、その仕組みは解明されていませんでした。光の吸収は色素の周辺環境の違いや構造の歪みによって大きく変わります。そこで私たちは、クライオ電子顕微鏡法を用いて、ミルの光合成アンテナの色素のタンパク質内での構造と結合環境を高分解能で解析することにより、青緑色光吸収を達成する分子メカニズムの解明につながる基礎的な情報を得ようと考えました。  図 1 海洋性大型緑藻ミル（*Codium fragile*)の写真 （上）とシフォナキサンチンの化学構造（下） <研究の内容> 本研究では、ミルの光合成アンテナの構造をクライオ電子顕微鏡により高分解能で取得し、シフォナキサンチンの構造とクロロフィル *b* の置換位置（602)を明らかにしました。 シフォナキサンチンは大きくねじれており、周囲のタンパク質と 2 カ所で水素結合を形成していることを明らかにしました。これらの構造的特徴はシフォナキサンチンが緑色光を吸収するようになる鍵となると考えられます。また、手法的に困難であったクロロフィル *a* とクロロフィル *b* の違いを検出することに成功し、クロロフ

	ィルの置換部位を一部明らかにしました。これによりクロロフィル *b* が隣接して並んだクラスターの領域が広くなり、青緑色光を効率よく光合成に利用する仕組みの解明に必要とされる色素の座標情報が得られました。 <期待される効果・今後の展開> 　青緑色光を光合成に活用する種は他にもあり、タンパク質の構造と光利用機構について盛んに研究されていますが、まだ完全には明らかになっていません。本研究で得られたミルの光合成アンテナの構造は、よく研究されてきた陸上植物の光合成アンテナと色素の構造だけが異なるため、青緑色光の吸収を可能とする原理を構造から解き明かす糸口となることが期待できます。 本研究で用いたミルは、万葉集の時代から知られる日本原産の食用海藻ですが、ここ 100 年の間に世界中の港に広がり、侵略的外来種としてはびこっています。これはさまざまな光環境に適応できる生命力の強さを示しています。したがってミルの光合成アンテナの構造に基づき、光環境適応の分子機構を解明することは、海洋の生態系を守る戦略につながると考えられます。 また、有機分子である色素の構造を制御することで吸収できる光の波長範囲（色）を広げる分子メカニズムは、太陽光のさまざまな波長の光を高効率で集積し、再生可能エネルギー源として用いるためのデバイスの設計にヒントを与えると思われます。 今後は、この色素がどのように青緑色光吸収を達成するかについて、生化学、構造生物学、分光学等のさまざまな手法を駆使することで、解明していく予定です。 ‘海中での光合成、どうすれば効率的？メカニズムの解明に光～クライオ電子顕微鏡法を用いて解析～’ 大阪公立大学. https://www.omu.ac.jp/info/research_news/entry-03405.html (参照 2022-12-05)
News	“Shedding light on photosynthesis at sea”. Osaka Metropolitan University. https://www.omu.ac.jp/en/info/research-news/entry-19936.html , (accessed 2022-12-14) The American Association for the Advancement of Science. “Shedding light on photosynthesis at sea”. EurekAlert!. https://www.eurekalert.org/news-releases/974262, (accessed 2022-12-14) “Shedding light on photosynthesis at sea”. Alpha Galileo. https://www.alphagalileo.org/Item-Display/ItemId/228562, (accessed 2022-12-14) “Shedding light on photosynthesis at sea”. Asia Research News. https://asiaresearchnews.com/content/shedding-light-photosynthesis-sea-0, (accessed 2022-12-14)

BBA Advances 2 (2022) 100064

Contents lists available at ScienceDirect

BBA Advances

journal homepage: www.sciencedirect.com/journal/bba-advances

Structural insights into blue-green light utilization by marine green algal light harvesting complex II at 2.78 Å

Soichiro Seki [a], Tetsuko Nakaniwa [b,1], Pablo Castro-Hartmann [c], Kasim Sader [c], Akihiro Kawamoto [b,d], Hideaki Tanaka [b,d], Pu Qian [c], Genji Kurisu [b,d], Ritsuko Fujii [a,e,f,*]

[a] Division of Molecular Materials Science, Graduate School of Science, Osaka City University, 3-3-138, Sugimoto, Sumiyoshi-ku, Osaka 558–8585, Japan
[b] Institute for Protein Research, Osaka University, Suita, Osaka 565–0871, Japan
[c] Materials and Structural Analysis, Thermo Fisher Scientific, Achtseweg Noord 5, 5651 GG Eindhoven, Netherlands
[d] Institute for Open and Transdisciplinary Research Initiatives (OTRI), Osaka University, Suita, Osaka 565–9871, Japan
[e] Department of Chemistry, Graduate School of Science, Osaka Metropolitan University, 3-3-138, Sugimoto, Sumiyoshi-ku, Osaka 558–8585, Japan
[f] Research Center for Artificial Photosynthesis (ReCAP), Osaka Metropolitan University, 3-3-138, Sugimoto, Sumiyoshi-ku, Osaka 558–8585, Japan

ARTICLE INFO

Keywords:
Codium fragile
Cryo-EM
Light-harvesting complex
Siphonaxanthin–chlorophyll *a*/*b*-binding protein (SCP)
Intermonomer chlorophyll *b* macrocluster

ABSTRACT

Light-harvesting complex II (LHCII) present in plants and green algae absorbs solar energy to promote photochemical reactions. A marine green macroalga, *Codium fragile*, exhibits the unique characteristic of absorbing blue-green light from the sun during photochemical reactions while being underwater owing to the presence of pigment-altered LHCII called siphonaxanthin–chlorophyll *a*/*b*-binding protein (SCP). In this study, we determined the structure of SCP at a resolution of 2.78 Å using cryogenic electron microscopy. SCP has a trimeric structure, wherein each monomer containing two lutein and two chlorophyll *a* molecules in the plant-type LHCII are replaced by siphonaxanthin and its ester and two chlorophyll *b* molecules, respectively. Siphonaxanthin occupies the binding site in SCP having a polarity in the trimeric inner core, and exhibits a distorted conjugated chain comprising a carbonyl group hydrogen bonded to a cysteine residue of apoprotein. These features suggest that the siphonaxanthin molecule is responsible for the characteristic green absorption of SCP. The replaced chlorophyll *b* molecules extend the region of the stromal side chlorophyll *b* cluster, spanning two adjacent monomers.

1. Introduction

Although sunlight is a renewable source of energy, its low photon density makes its use as a source of chemical energy difficult. Photosynthetic organisms have developed light-harvesting systems that collect and supply energy to photosynthetic reaction centers [1]. However, sunlight occasionally becomes sufficiently intense to cause damage (similar to an overdose) to photosynthetic systems [1,2]. Thus, photosynthetic organisms are required to not only use sunlight efficiently (light harvesting) but also compensate during overdose circumstances via a rapid energy dissipation system (excess energy quenching) [1,2]. Rapid energy dissipation mechanisms are collectively termed as non-photochemical quenching (NPQ), which is dominated by energy-dependent quenching (qE) [2]. In plants, light-harvesting complex II (LHCII) is critical in light harvesting and excess energy quenching [2]. Atomic resolution X-ray structure analyses [3,4] have provided accurate coordinates of the pigments bound to the plant-type LHCII. Each monomeric protein contains the following molecules: eight chlorophyll (Chl) *a*, six Chl *b*, two lutein, one 9′-*cis* neoxanthin (Nx), and one violaxanthin. The function of LHCII in photosynthesis has been spectroscopically examined, and several excitonic models have been proposed [5,6] to explain the primary features of the spectroscopic results

Abbreviations: C., *Codium*; Chl, chlorophyll; cryo-EM, cryogenic electron microscopy; CTF, contrast transfer function; EMDB, Electron Microscopy Data Bank; HPLC, high-performance liquid chromatography; LHCII, light-harvesting complex II; LHCSR, light-harvesting complex stress related protein; NPQ, nonphotochemical quenching; Nx, 9'-*cis*neoxanthin; PDB, Protein Data Bank; PG, dipalmitoylphosphatidylglycerol; qE, energy-dependent quenching; SCP, siphonaxanthin–chlorophyll*a*/*b*-binding protein; S_{ICT}, intramolecular charge-transfer; Sn, siphonein; Sx, siphonaxanthin; lut2, lutein at the L2 site.

* Corresponding author.
E-mail address: ritsuko@omu.ac.jp (R. Fujii).
[1] Present address: StemRIM Inc., Saito Bio-Incubator 3F 7-7-15, Saito-Asagi, Ibaraki City, Osaka 567–0085, Japan.

https://doi.org/10.1016/j.bbadva.2022.100064
Received 20 August 2022; Received in revised form 9 November 2022; Accepted 9 November 2022
Available online 11 November 2022

[2,7,8], although some questions remain [2,5,8,9]. For NPQ generation, several mechanisms have been proposed based on local interactions of Chl-Chl and Chl-carotenoid in LHCII, but whether they fully explain the experimental results is under debate, and no consensus has been reached [2,5,10]. To further elucidate the mechanism of these functions, it is promising to apply advanced spectroscopic techniques to pigment-altered LHCII based on high-resolution structural data [2,5,9].

Marine macroalgae constitute the primary producers of organic carbon in coastal ecosystems and contribute to the global sequestration of atmospheric carbon in deep sea owing to their rapid growth in numerous habitats [11]. Siphonous green macroalgae, a group of marine macroalgae, grows well in the intertidal zone [12] where sunlight conditions change regularly and sometimes drastically, from weak blue-green light to intense white light, depending on the water depth [13]. Among various siphonous green macroalgae, *Codium (C.) fragile,* which is native to Japan but has invaded intertidal ecosystems in harbors worldwide over the past century [12], contains a unique LHCII that efficiently utilizes the blue-green light available underwater [14–18]. This is because of the pigments bound to LHCII: carbonyl carotenoids siphonaxanthin (Sx) and siphonein (Sn), which are substituted with two lutein molecules, absorb green light, and a high proportion of Chl *b* molecules induces a larger absorption cross section for blue light [14,15]. This is collectively referred to as the Sx–Chl *a/b*-binding protein (SCP) [14]. However, siphonous green algae do not exhibit qE-type NPQ [19]. Moreover, as they lack photoprotective light-harvesting complex-family proteins (LHCSR and PSBS) and a light-dependent Chl biosynthetic enzyme, the photoprotective mechanisms of siphonous green algae remain largely unknown [20].

SCP differs from spinach LHCII in two aspects: a 2-nm blueshift of the fluorescence peak and the presence of the so-called long-lived Chl *b* responsible for an additional Qy absorption peak at 659 nm between the well-characterized Qy bands of Chl *b* and Chl *a* in the spinach LHCII. Moreover, recent two-dimensional electronic [21,22] and single molecular [23,24] spectroscopic observations have indicated that SCP demonstrates drastically different excitation energy dynamics from those of spinach LHCII. Recently, the pigment composition of SCP, especially of carotenoids, was found to be significantly altered in *C. fragile* depending on the intensity and color (wavelength) of the irradiated light during culture [25]. Particularly, blue-green light enhances the substitution of Sx and Sn in SCP with lutein and 19-deoxysiphonaxanthin [25]. Similar changes in pigment composition due to high-intensity light irradiation have been reported for a naturally occurring siphonous green alga, *Caulerpa racemosa* [26], and a photoacclimation mechanism involving Sx–lutein interconversion has been proposed [25,26]. However, the lack of information regarding the structure of SCP limits further discussion.

Here, we determined the cryogenic electron microscopy (cryo-EM) structure of SCP, purified from *C. fragile* grown in dim light to avoid heterogeneity in carotenoid composition, at a resolution of 2.78 Å. The locations of Sx, Sn, and the two substituted Chl *b* molecules in SCP were determined. The structural differences from spinach LHCII were primarily detected in the periphery of the SCP trimer. In this study, we described the main differences from the spinach LHCII that appeared in SCP, which could affect the energy dynamics.

2. Materials and methods

2.1. Sample preparation

SCP was purified from laboratory cultivated *C. fragile* (KU-0654, KU-MACC, Kobe, Japan) in a filamentous form as described in ref [25]. Briefly, the crude SCP band collected from the initial sucrose density gradient was purified twice using an ion exchange column chromatograph and collected again by the sucrose density gradient centrifugation. After final purification with a gel filtration column, the resultant SCP solution was concentrated to be ~7.0 mg ml^{-1} and frozen at 77 K until use.

2.2. Spectroscopy

Optical spectra, namely absorption, fluorescence and fluorescence excitation, and circular dichroism spectra were recorded in 20 mM Tris-HCl pH 8.2 containing 0.03% β-DDM using UV-1800 (Shimadzu, Kyoto, Japan), FP-8500 (JASCO, Tokyo, Japan), and J720W (JASCO, Tokyo, Japan), respectively (SFig. 1a−b).

2.3. High-performance liquid chromatography (HPLC) analysis

All pigments were extracted from whole cells or purified SCP, and subjected to the HPLC system as described in ref [25]. Briefly, whole pigments were extracted from a lyophilized sample and then re-dissolved into dimethyl formamide. HPLC analyses were performed using an ODS column (Cosmosil $_{2.5}C_{18}$-MS-II, 2.0 mm ID x 75 mm, Nacalai tesque, INC., Kyoto, Japan) and detected by a photodiode array detector (SPD-40M, Shimadzu, Kyoto, Japan) using gradient elution. Pigment compositions were calculated using the molar extinction coefficient given in [25,27]. The standard errors were calculated from three biological replicants (SFig 1c).

2.4. Cryo-EM data collection

A 3.0 μl aliquot of the purified SCP (~7.0 mg ml^{-1}) was applied to a glow-discharged holey carbon grid (Quantifoil grid R1.2/1.3, 300 mesh Cu). The grid was plunged into liquid ethane cooled by liquid nitrogen using a FEI Vitrobot 4 under a following condition: blotting time 2.5 seconds, blotting force 1, sample chamber humidity 99%, sample chamber temperature 4 °C. The frozen grid was stored in liquid nitrogen before use. Data were recorded on a Thermofisher Scientific Titan Krios G3i Cryo-EM equipped with a Falcon 4 direct electron detector at the Cambridge Pharmaceutical Cryo-EM Consortium [28]. The microscope was operated at 300 kV accelerating voltage and a nominal magnification of 120 k, corresponding to a pixel size of 0.65 Å at the specimen level. The detector was operated in a counting mode. The total dose of 50.75 electrons per Å^2 was fractionated on 42 frames within 10 seconds of exposure time, resulting in a unit area electron dose of 1.21 electrons per Å^2 per frame. In total, 8935 movies were collected with defocus values varying from 0.8 to 2.2 μm using aberration-free image shift protocol (AFIS). Typical cryo-EM images averaged from motion-corrected movie frames are shown in SFig. 2.

2.5. Cryo-EM data processing

The movie frames were subsequently aligned to correct for beam-induced movement and drift using MotionCor2 [29], and the contrast transfer function (CTF) was evaluated using Gctf [30]. In total, 2,336,076 particle images were automatically picked from 8,250 images using Gautomatch (http://www.mrc-lmb.cam.ac.uk/kzhang/), and then several rounds of 2D classifications were performed using RELION-3.1 [31]. A total of 1,807,516 particles were selected for building the initial model of the SCP using cryoSPARC2 [32] and subjected to 3D classification into 10 classes using RELION-3.1 (SFig. 2). The best 3D class representing a trimmer SCP was selected for further refinement. In total, 250,633 particles were re-extracted with a pixel size of 0.65 Å/pixel and subjected to five 3D refinements, three CTF refinements, and Bayesian polishing. For the cryo-EM images of SCP, the movie frames were collected using two different cryo-EM. Since the pixel size is slightly different, the pixel size was corrected using the value of the anisotropic magnification estimated by the CTF refinement process. The corrected pixel size value was 0.662 Å/pixel. Final 3D refinement and post-processing yielded maps with global resolutions of 3.13 Å (C1) and 2.78 Å (C3), according to the 0.143 criterion of the FSC. No obvious difference could be observed between the C1 and C3 maps in terms of

structural features. Since the C3 symmetrized map reduced noise level, it was used for model building. The local resolution was estimated using RELION-3.1. The processing strategy is described in SFig. 2.

2.6. Modeling and refinement

The atomic model of SCP was constructed with using WinCOOT 0.9.447 [33], Phenix 1.19-415848 [34], and both Chimera and ChimeraX [35] software packages. The coordinate of spinach LHCII (PDB: 1RWT) was directly docked as a template into the C3 symmetry imposed cryo-EM map of SCP using Chimera such that the trans-membrane helices were roughly matched to the electrostatic potential profile of the cryo-EM map. Amino acids in the template were replaced one by one using WinCOOT to fit the SCP sequence (DDBJ: LC536571). Then a rigid body refinement was performed in Chimera, forming an atomic model of the SCP. CIF files for Sx and Sn were constructed, and two lutein molecules were replaced with Sx and Sn, respectively, in WinCOOT to match the cryo-EM derived density profile (which is referred to simply as the density hereafter). Each Chl molecule obtained from the template was examined for its density to determine whether it matched Chl *a* or Chl *b* molecule, and two Chl *a* molecules (602 and 610) were replaced with Chl *b* molecules in WinCOOT. After real space refinement in WinCOOT, the geometry-optimized model was globally refined in Phenix to achieve a global resolution of 2.73 Å. After further refinement to acquire better density around Chl molecules, the global resolution became slightly poor to be 2.78 Å in the final density map. The refinement statistics are summarized in supporting material (STable 1). The refined model and its cryo-EM map were deposited in the Protein Data Bank (PDB) and the Electron Microscopy Data Bank (EMDB) with codes 7WLM and EMD-32588, respectively.

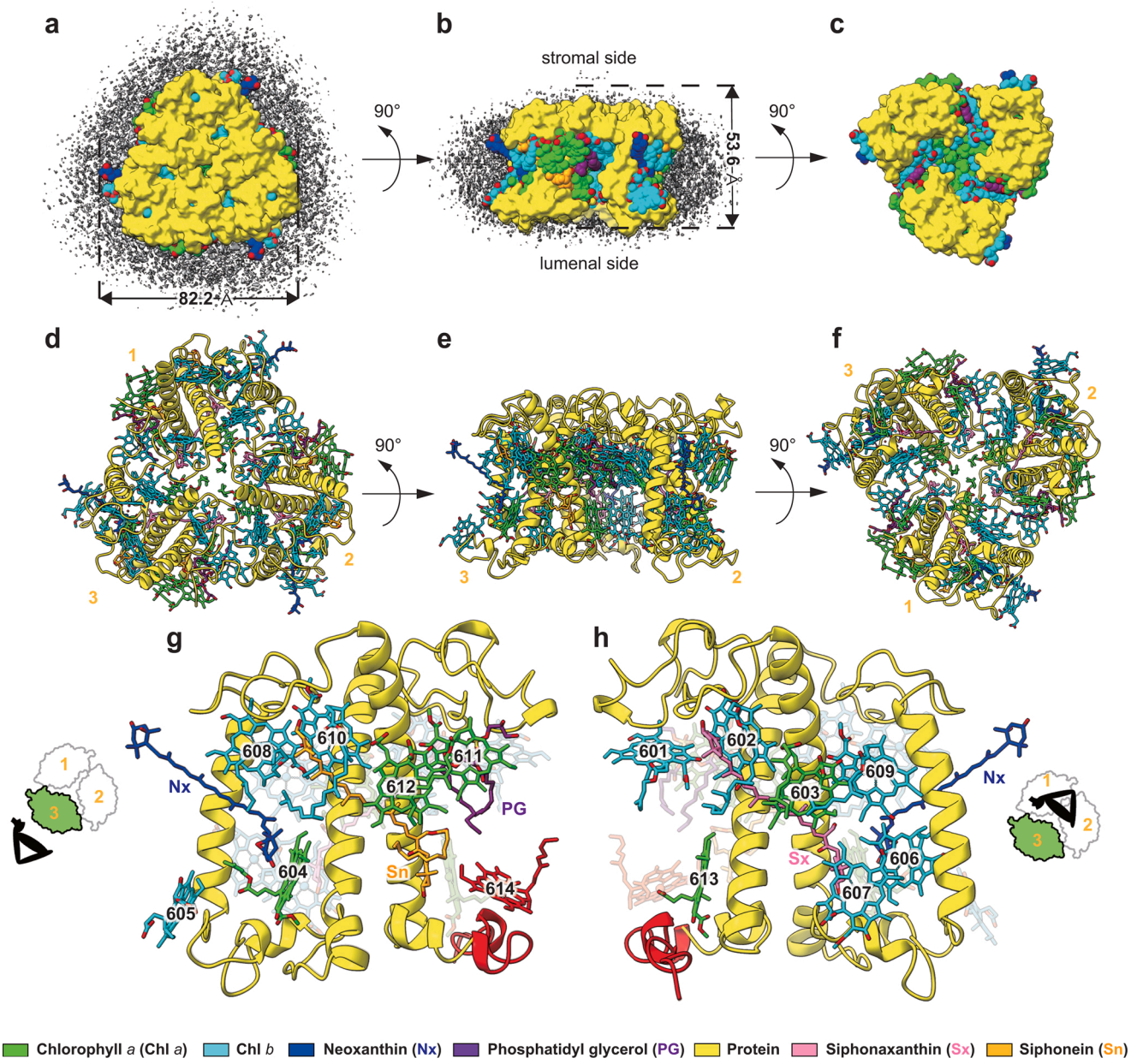

Fig. 1. Cryo-EM structure of SCP.
Panels **a**–**c** show the SCP model surface on the cryo-EM map. Panels **d**–**h** show the model coordinates with cofactors. Panels **a** and **d** are viewed from the stromal side, panels **b** and **e** from the membrane plane, and panels **c** and **f** from the lumenal side. Each monomer is numbered from 1 to 3 in panels **d**–**f.** Panels **g** and **h** show the side views of a monomer from the outer (left) and the inner (right) sides of the trimer, respectively. The red parts represent missing densities displayed against the structure of spinach LHCII (1RWT). The figures were drawn using ChimeraX [35].

2.7. Peptide fingerprint analyses of the C terminus of SCP

Peptide mass fingerprint analyses were performed for the SCP band after SDS-PAGE gel. In-gel digestion was performed by Digest Pro 96 (INTAVIS Bioanalytical instruments AG, Cologne, Germany) with trypsin (Sequencing Grade Modified Trypsin, Promega Corporation, Madison, WI, USA). A concentrated peptide solution was placed onto MALDI AnchorChip Targets (Bruker), and then performed MALDI-MS measurements using Autoflex Speed (Bruker, Germany). Digested peptides were assigned using Biotools ver 3.2 (Bruker) according to the SCP amino acid sequences (Lhcbm11 and Lhcbm10, DDBJ: LC536571 and LC536572, respectively). Peptide sequences for two peptide ions in the C-terminal region were assigned using MS/MS measurements (LIFT) (see SFig. 3).

3. Results and discussion

3.1. Overall structure and pigment assignment

A functionally intact SCP was prepared from cultivated *C. fragile* (SFig. 1). An electron potential map of SCP was reconstructed at a global resolution of 2.78 Å from 8935 cryo-EM movies of 250,633 particles (SFig. 2) (Fig. 1a–f). SCP is a trimer with a molecular weight of 118 kDa. Each monomer comprises an apoprotein (223 amino acids), pigments (3 carotenoid and 14 Chl molecules), and a lipid molecule (assuming dipalmitoylphosphatidylglycerol [PG]). We sequenced the cDNA of five lhcb-family proteins from *C. fragile* and identified that two proteins, Lhcbm11 and Lhcbm10, constitute the SCP trimer using peptide mass fingerprinting analysis (SFig. 3). The apoprotein in the cryo-EM map was determined to be Lhcbm11 as its density profile fits better with the amino acids of Lhcbm11 than with those of Lhcbm10 at three specific positions unique to each sequence (SFig. 4b, c). Starting from the N-terminus (Ile 1) at the stromal side, three transmembrane (A, B, and C) and two amphipathic (D and E) helices were observed in the order of B, E, C, A, and D (Fig. 1g, h). The density profile continued to the His 201 residue in the center of helix D. However, the peptide chain continues up to a Phe 223 residue, the C-terminus (SFig. 3). Although the apoprotein likely continues to the C-terminus, it is hard to directly identify it in the cryo-EM map owing to its high flexibility.

The cryo-EM map indicates the presence of 3 carotenoid molecules and 13 Chl molecules in the monomer. The Chl molecules were named after the spinach LHCII [3]. The carotenoid molecules were determined to be Sx, Sn, and Nx based on the cryo-EM map and HPLC analyses (SFig. 1c). The carotenoid-binding sites corresponded well to those of spinach LHCII: Sx binds to the inner core of the trimer corresponding to the L2 site in spinach LHCII, while Sn binds to the periphery of the trimer corresponding to the L1 site in spinach LHCII (Fig. 1g, h). For clarity, the Sx and Sn binding sites have been referred to as SxL2 and SnL1, respectively. The cryo-EM map clearly demonstrates the s-*cis* conformation of the carbonyl group for the polyene backbone of both Sx and Sn (SFig. 5a, b). The locations and structures of the hydroxymethyl and acyloxy groups of Sx and Sn, respectively, were clearly identified in the cryo-EM map. Notably, the amount of Sx and Sn decreased slightly during the purification process (SFig. 1c). One plausible reason for this is that the presence of the V1 site in the natural environment (see below) allows SCP to bind an additional Sx or Sn to this site. However, it was difficult to identify a carotenoid in the V1 site on the cryo-EM map. Nevertheless, biochemical analysis detected a trace amount of violaxanthin, which often occupied the V1 site in plant-type LHCII, in *C. fragile* unlike purified SCP (SFig. 1c).

The cryo-EM map indicated the presence of 13 Chl macrocycles located in the transmembrane region with a relatively high local resolution (SFig. 2d and SFig. 4a). Despite the intrinsic difficulty in distinguishing Chl *a* and Chl *b* in the cryo-EM map [36,37], we identified 11 Chl molecules: 4 Chl *a* (603, 611, 612, 613) and 7 Chl *b* (601, 602, 605, 606, 607, 608, 609) molecules (SFigs. 6 and 7b). For example, the Chl at site 602 was determined to be Chl *b* based on the presence of a distinct density profile of the C7 formyl oxygen (SFig. 7b). For the remaining two sites (610 and 604), the density profile indicated a protrusion from the 7^1 carbon toward the formyl oxygen when the cutoff level fully covered the macrocycle (SFig. 7c and d, left panels). However, after lowering the cutoff level, the protrusion remained only in Chl 610 and not in Chl 604 (SFig. 7c and d, middle and right panels). Additionally, the cutoff level of Chl 604 was lower than that of Chl 610, indicating that the former exhibited a lower local resolution (SFig. 7a). Overall, site 610 appeared to be occupied by Chl *b*; however, a map of a higher resolution is required for conclusive determination. In SCP, the amino acid residues at sites 602 and 610 are well conserved with those in spinach LHCII (SFig. 8) and do not provide additional hydrogen bonds to the C7 formyl oxygen of the Chl *b* molecules. Moreover, these sites are exclusively occupied by Chl *a* molecules in various LHC-family proteins, such as the green lineage Lhcb and Lhca proteins [38] and the diatom Lhcf protein [39].

The Chl *a*/*b* ratio of purified SCP was determined to be ~0.71. This value lies between the ideal ratio of 0.75 (Chl $a/b = 6/8$) and 0.625 (Chl $a/b = 5/8$) (SFig. 1c), suggesting that some SCP lost one Chl *a* molecule after purification, consistent with the poor density profile corresponding to Chl 614 in spinach LHCII (indicated with red in Fig. 1g, h). Because the axial ligand (His 201) of Chl 614 was conserved in SCP, the unidentified site 614 in SCP could be occupied by a Chl *a* molecule.

Based on direct hydrogen bonds with cofactors (4 Chl and 1 PG molecules) and the hydrogen bond networks involved, 18 water molecules were identified. Owing to the difficulty in distinguishing water molecules from noise on the cryo-EM map [40], the X-ray crystal structure of spinach LHCII [3] was used as a reference to identify water molecules in SCP.

The overall structure of the apoprotein is almost identical to that of spinach LHCII [3], with a few differences (Fig. 2 and SFig. 8a). The Tyr 76 residue inserted at the lumenal terminus of helix B introduced a small expansion toward the outer side of SCP (Fig. 2a). The insertion of a Glu 17 residue into the N-terminal loop forced two neighboring residues to expand, protruding toward the adjacent monomer and deforming the stromal terminus of helix C (helix C' in Fig. 2b). Replacing a Trp residue with a Phe residue in a part of the "trimerization motif" could reduce the hydrophobic steric hindrance and correspondingly the repulsive force toward the hydrophilic headgroup of PG (Fig. 2c) [41]. Replacing two Leu residues with Phe in a part of the so-called "carotenoid-binding motif" [42] (Fig. 2d) and a Leu residue with a Trp residue at the center of helix D (Fig. 2e) increases hydrophobicity, stabilizing the hydrophobic Sn from both ends (See below). The outer surface of the SCP trimer, which governs the interaction of other proteins within the thylakoid membranes, was almost identical to that of spinach LHCII [3], except for a small protrusion on the lumenal side of helix B (Fig. 2a). In spinach LHCII, a Trp residue in helix C' faces the V1 xanthophyll, whereas in SCP, the corresponding Trp 118 residue is oriented in a different direction because it is shifted one residue toward the C-terminus (SFig. 8a). Conversely, the geometric relationship of helix C' in the trimer agrees well with that of spinach LHCII (Fig. 2f). This suggests that SCP has a V1 carotenoid-binding pocket with a different binding affinity from that of spinach LHCII.

3.2. Structures of Sx and Sn and their binding environments

Sx and Sn have a carbonyl group asymmetrically attached to the polyene backbone (SFig. 5). Such carbonyl carotenoids can form an intramolecular charge-transfer (S_{ICT}) state [43,44]. For peridinin and fucoxanthin bound to the light-harvesting complex, the S_{ICT} state is well-characterized and allows highly efficient energy transfer to Chl *a* [7,43,44]. All fucoxanthin molecules exhibit s-*trans* conformation in the light-harvesting complexes of diatoms [39,45], different from the s-*cis* conformation of both Sx and Sn in SCP. However, the influence of the s-*cis* or s-*trans* conformation on optical properties remains unclear [46].

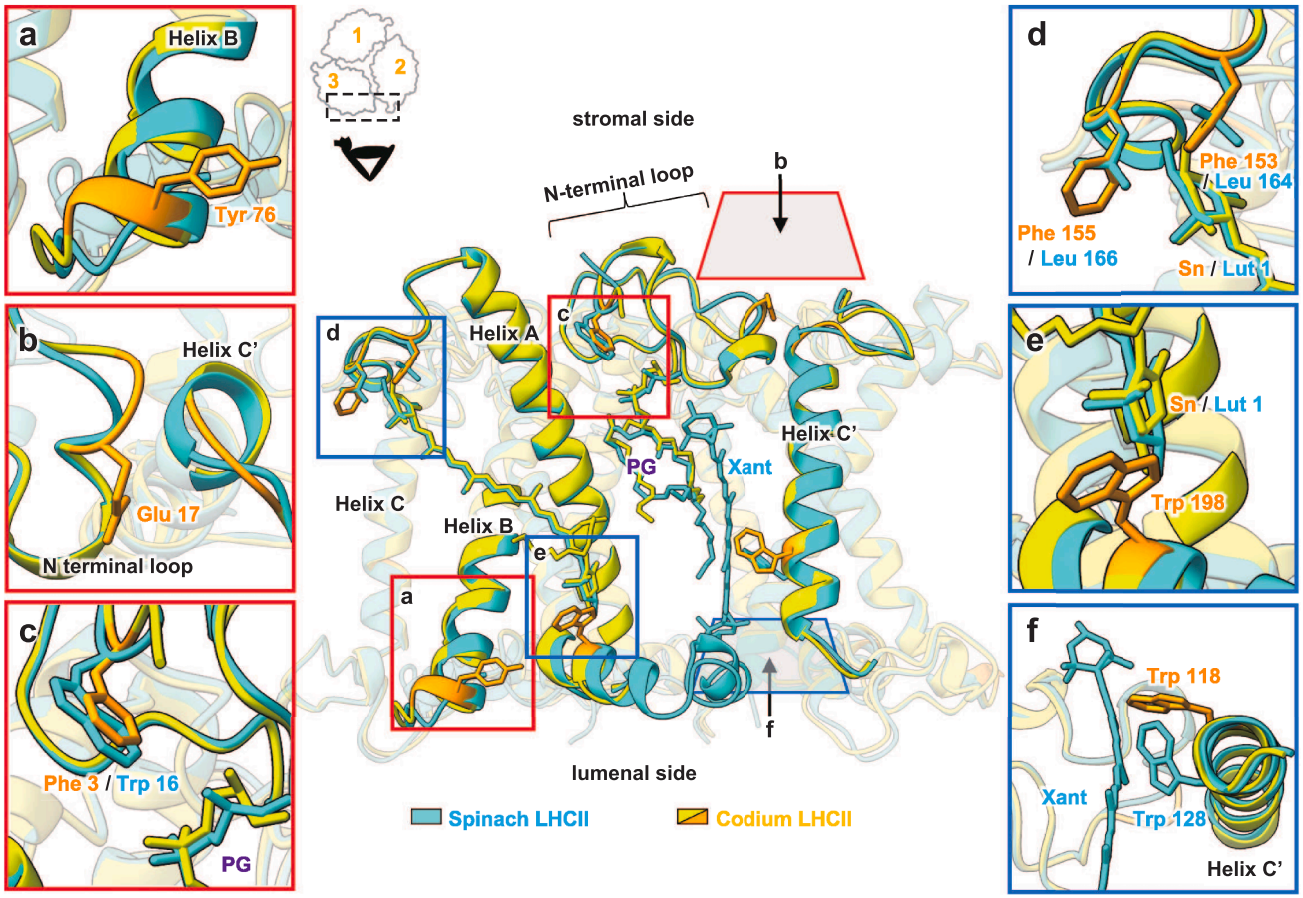

Fig. 2. Differences in coordinates between spinach LHCII and *Codium* SCP: enlarged views from the boxed windows (**a**–**e**).
Coordinates of spinach LHCII (cyan, 1RWT) and *Codium* SCP (yellow, 7WLM) were superimposed based on the A, B, and C helices using CCP4MG version 2.10.11. Panels **a**–**f** show enlarged views: **a,** lumenal edge of the helix B; **b,** proximal region of the N-terminal loop and helix C of the neighboring monomer; **c,** trimeric motif with proximal PG; **d, e,** around the 3′- and 3-hydroxy end-rings of the carotenoid, respectively; and **f,** a vertical projection from the lumenal side of the helix C' adjacent to a xanthophyll (Xant) associated with spinach LHCII. The figures were drawn using ChimeraX [35].

Comparing the Sx and Sn binding sites revealed that the SnL1 site of the latter is more hydrophobic than the SxL2 site of the former owing to the accumulation of the nonconserved amino acid residues at the SnL1 site (Fig. 3 and SFig. 8a). Nonconserved hydrophobic residues appear at the intervals of one or two residues in helix B (Val 64, Val 65, and Leu 68), in the middle of the stromal loop between helices C and A (Phe 153 and Phe 155), and in the middle of the lumenal amphipathic helix D (Trp 198) (SFig. 8a). These residues face Sn, generating a large hydrophobic cavity, which helps to preferentially and stably retain a bulky hydrophobic carotenoid. Conversely, the amino acid residues that face Sx are conserved (Fig. 3b). A relatively hydrophilic belt is observed on the protein surface of the SxL2 site along the Sx molecule because of the absence of hydrophobic side chains directed toward Sx (Fig. 3e). Furthermore, the C7 formyl oxygen of Chl *b*602, located between the protein surface and Sx, is proximal to the conjugate plane of Sx (Fig. 3e, Fig. 4c). Thus, we conclude that the SxL2 site is relatively hydrophilic and polarized. Since polar solvents promote the S_{ICT} characteristics of carbonyl carotenoids [43,44,47], Sx at the SxL2 site is expected to exhibit stronger S_{ICT} characteristics than Sn at the hydrophobic SnL1 site.

Sx accepts two newly introduced hydrogen bonds from the backbone of Trp 59 and the thiol group of Cys 67 to the 19-hydroxymethyl and the 8-carbonyl groups, respectively, in addition to the hydrogen bonds of the hydroxy groups at the rings at both ends (Fig. 3c). The observed distance of 3.6 Å between a sulfur atom of Cys 67 and the carbonyl oxygen of Sx was slightly longer than the typical hydrogen bond lengths (2.7–3.3 Å) but reasonable in terms of hydrogen bond lengths between a Cys residue and carbonyl group (3.5 ± 0. 22 Å between O and S atoms [48]). Trp 59 is highly conserved among other light-harvesting complex-family proteins, such as lhca and lhcb, whereas Cys 67 is only conserved among the trimeric lhcb proteins in vascular plants [38]. The resonance Raman spectra of SCP differed significantly from those of spinach LHCII [18]. Specifically, when excited at 441.6–488.0 nm, SCP presents a unique band at 1623 cm^{-1} in a fingerprint region of C=O stretching vibrational modes from hydrogen-bonded carbonyl groups. As Sx, Sn, as well as Chl *b* contribute to resonant absorption in this wavelength region, this signal probably originates from the hydrogen-bonded 8-carbonyl group of Sx. Akimoto et al. [16,49,50] suggested that the unusual fluorescence anisotropy of the green band is attributable to the hydrogen bonding to the 8-carbonyl group of Sx. This observation is consistent with our findings.

Sx at the SxL2 site is distorted from C9′ to C7′ compared with Sn at the SnL1 site (Fig. 3f and SFig. 5c). The steric hindrance of Chl *a*603′ from the neighboring monomer may cause this distortion, as observed in spinach LHCII [51,52]. This is consistent with the results of resonance Raman spectroscopy wherein two nonequivalent Sx-type molecules resemble the optical behavior of two lutein molecules of spinach LHCII [18]. Therefore, we conclude that the redshifted absorption band at ~535 nm is due to Sx at the SxL2 site while the band at ~501 nm is due to Sn at the SnL1 site.

Furthermore, the conjugated chains of both Sx and Sn face the macrocycles of Chl *a*603 and *a*612 and Chl *b*602 and *b*610, respectively

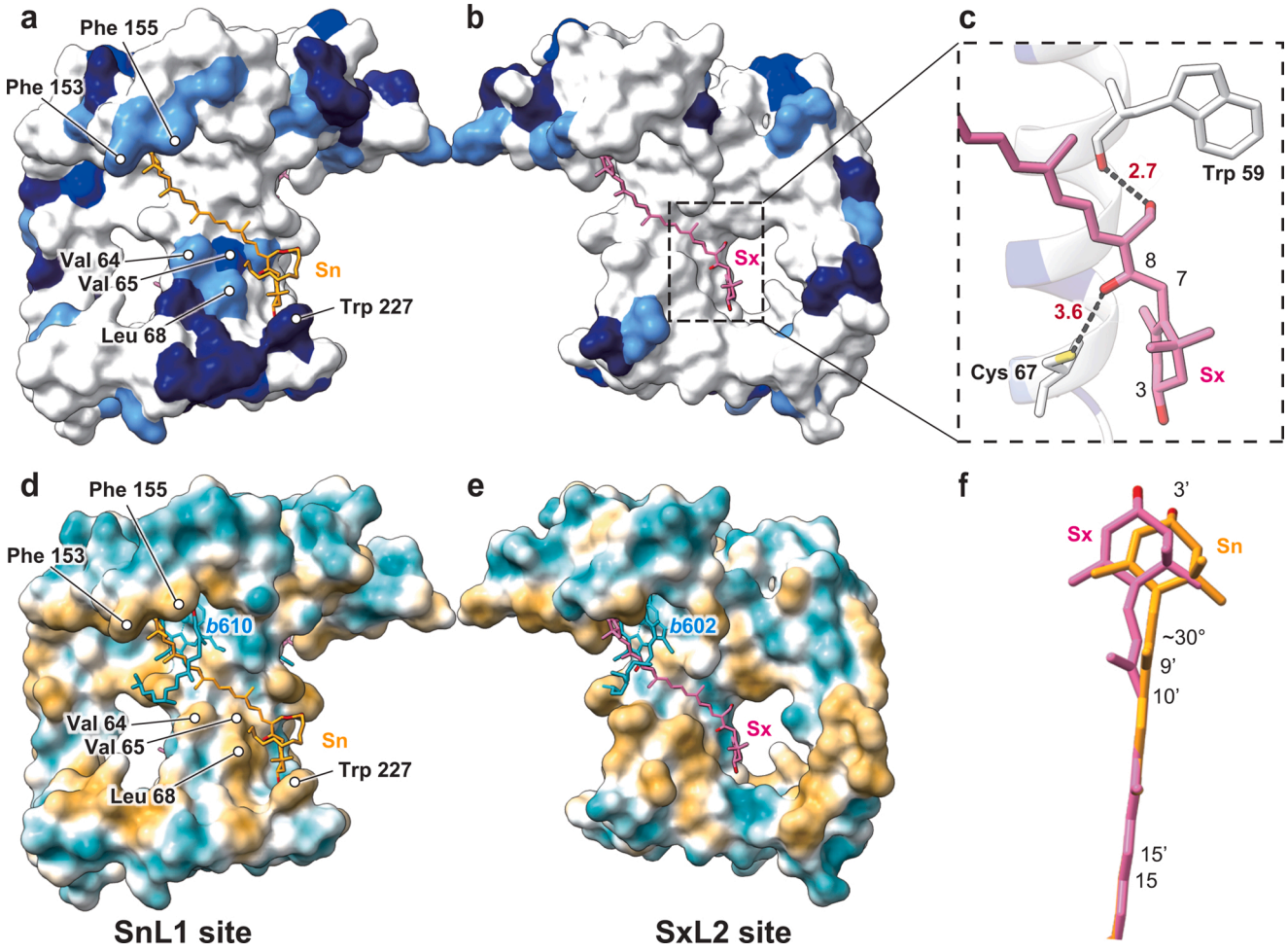

Fig. 3. Siphonein (Sn) and siphonaxanthin (Sx) binding pockets (**a**–**e**) and their conformations (**f**).
Panels **a, b, d**, and **e** show the SCP model surfaces of the carotenoid-binding pockets of Sn (**a** and **d**) and Sx (**b** and **e**). Amino acid residues are color coded for **a** and **b,** homology to spinach LHCII (white, conserved; cornflower blue, strongly conserved; blue, weakly conserved; and midnight blue, not conserved, as in SFig. 8), and for **d** and **e,** polarity (yellow, hydrophobic; blue, hydrophilic), respectively. Panel **c** represents the enlarged view of the area enclosed by the dashed square in **b**. The hydrogen bonds are shown in broken lines with distances in Å. Panel **f** represents coordinates of Sx and Sn superimposed at the central part of the molecule (C10−C10′ and methyl groups therein). In **d** and **e**, Chl *b*610 and *b*602 are shown, respectively. The figures were drawn using ChimeraX [35].

(Fig. 4). At distances of 3.8-3.4 Å, strong dipole interactions enhance the excitation energy transfer between them. Hence, Sx at the SxL2 site primarily absorbs green light and efficiently transfers the energy to Chl molecules through the S_{ICT} state. Further experiments are warranted to clarify this hypothesis.

Since the SxL2 site of SCP is identical to the L2 site of LHCII to which lutein binds, SCP can likely accept lutein at its SxL2 site. This is consistent with previous findings stating that lutein binds to SCP when the algae are grown under intense blue-green light [25]. Additionally, lutein at the L2 site (lut2) has been proposed as a quenching site in spinach LHCII [2,52], suggesting that lutein binding to SCP instead of Sx may contribute to mitigating photodamage through quenching.

3.3. *Plausible generation of the intermonomeric macrocluster of Chl b at the stromal side*

The structure of SCP revealed that Chl *b* molecules replaced Chl *a* molecules at sites 602 and 610 on the stromal side. However, all Chl arrangements, including the Mg–Mg distance and dipole orientation (Fig. 4a), were nearly identical to those in spinach LHCII [3]. The excitation energy transfer between Chl molecules in spinach LHCII has been well described by the concept of Chl clusters [8]. The replaced Chl *b* molecules approach from both sides of the *b*608-*b*609-*b*601′ cluster defined for spinach LHCII [5,8], expanding the area of the Chl *b* cluster (Fig. 4b). The resultant Chl *b* macrocluster (610-608-609-601′-602′) spans two adjacent monomers, potentially contributing to trimer-specific energy transfer.

The Qy band energy of each Chl molecule bound to LHCII shows a specific shift from that in organic solvents due to the environmental heterogeneity of each binding site, called site energy [8]. In spinach LHCII, the calculated site energies for both 602 and 610 show a large redshift [5,6,9]. The charged residues in those binding sites, mainly responsible for the site energy shift [6], are identical to those in spinach LHCII [3] (SFig. 8). Therefore, in SCP, the extent of the redshift of the site energies of both Chl molecules at sites 602 and 610 should remain the same. Consequently, in SCP, *b*602 and *b*610 exhibit the lowest Qy energy in the Chl *b* macrocluster. Besides forming the Chl *b* macrocluster, the strongly excitonically coupled Chl *a* dimer (611–612) and relatively isolated Chl *a* (603) remain (Fig. 4b). Hence, a plausible picture is that the initially delocalized excitation energy in the Chl *b* macrocluster is transferred via the low-energy Chl *b* molecules (602 and 610) to adjacent Chl *a* molecules (603 and 612), respectively. The long-lived Qy state of Chl associated with absorption at 659 nm detected by low-temperature absorption [18,21,53] and two-dimensional electronic spectroscopy [21] of SCP has recently been proposed to be due to a weakly-coupled excitonic state between Chl *b* and Chl *a* molecules [22].

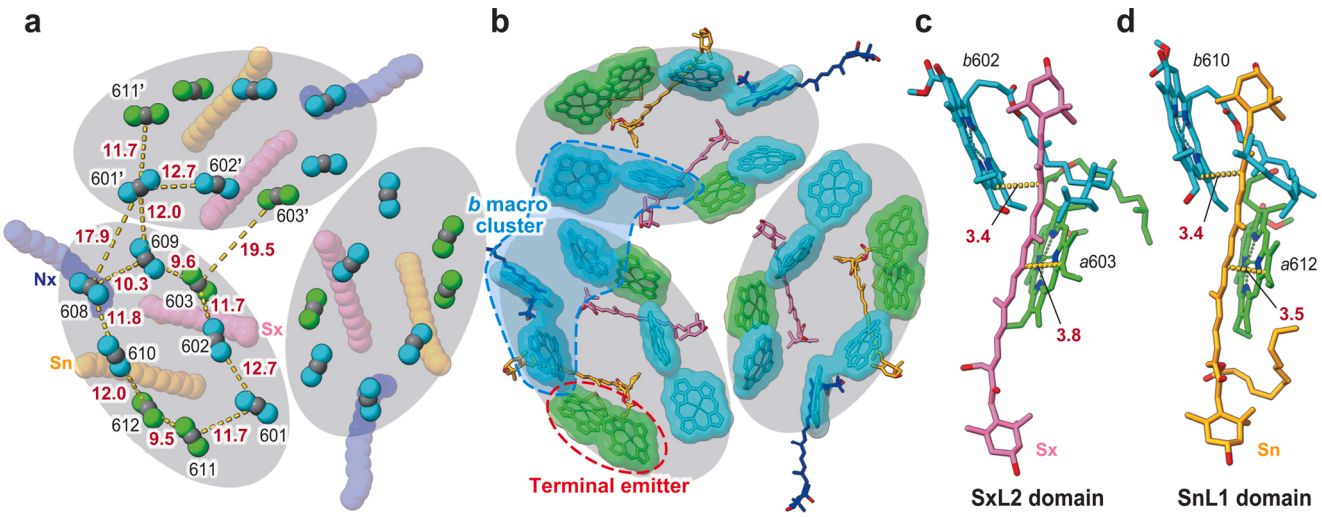

Fig. 4. Pigment arrangements at the stromal side of the trimer (**a, b**), and around the carotenoids (**c, d**).
Panels **a** and **b** represent the pigment coordinates of SCP from the stromal side. **a**, Each Chl molecule is indicated by a central Mg atom (gray) and two nitrogen atoms (lime green for Chl *a* and cyan for Chl *b*) along the Qy axis. The distances between the Mg atoms are shown in bold in Å. **b,** Putative Chl clusters are enclosed by broken lines (see text). Panels **c** and **d** represent the coordinates of Sx and Sn with the proximal Chl molecules: the closest C–C distances between each Chl macrocycle and the conjugated carbon of Sx or Sn are shown in bold in Å. The figures were drawn using Chimera X [35].

This would correspond to the two candidate pairs: the *b*602–*a*603 pair and/or the *b*610–*a*612 pair in SCP. Thus, SCP exhibits significantly different Chl clustering on the stromal side than spinach LHCII.

Another spectroscopic feature of SCP is the 2-nm blueshift of its emission maximum compared with that of spinach LHCII (SFig. 1a). The Chl *a* cluster of 610–611–612 has been attributed as the terminal emitter of spinach LHCII at the stromal side [2,5,6,9]. This cluster forms the *a*611–*a*612 dimer in SCP (Fig. 4b). The blueshift of absorption is thus attributable to the change from the Chl *a* cluster (610-611-612) to the Chl *a* dimer (611-612). However, this observation somewhat differs from that of Nguyen et al. [22]. Using spinach LHCII-based exciton models with all possible combinations of Chl *a*-to-*b* two-site substitutions, they concluded that only the substitution pair of 602 and 611 or 612 represents the blueshift of the terminal emitter and that the substitution pair of 602 and 610 does not induce a sufficient blueshift [22]. The calculated site energy is highly dependent on assumptions such as the methodology and environmental factors [7,9], and spinach LHCII-based exciton models do not include the influence of Sx and Sn, which have static dipoles and potentially large transition dipoles. Therefore, further calculation using an elaborate model based on the structure determined here is warranted to solve this slight discrepancy.

Notably, despite the apparent lack of qE-type NPQ in species containing SCP [19], some of the proposed quenching sites for spinach LHCII [2,8] are conserved in SCP, i.e., the *a*603–*b*609 and *a*613–*a*614 pairs. Recently, we applied single-molecule spectroscopy to SCP [24] and observed that the single SCP exhibited a signal that somewhat resembled the "moderately redshifted" emission observed in a single spinach LHCII. This signal was observed when excited at 639 nm but not at 561 nm and was associated with a substantially reduced lifetime [24]. To explain the redshifted emission observed in the single LHCII, Krüger et al. proposed switching between two quenching sites in the lut2-*a*603-*b*609 and lut1-*a*610-*a*611-*a*612 domains of spinach LHCII by changing the protein conformation [8,54]. The applicability of this model to SCP will be examined in follow-up experiments that are currently underway. The newly determined structure of SCP may be beneficial in improving the understanding of and give new insight into the quenching mechanism of the trimeric LHCII framework.

4. Conclusion

We successfully determined the three-dimensional (3D) structure of SCP from *C. fragile* at 2.78 Å resolution using cryo-EM. The overall 3D structure of SCP is almost identical to that of spinach LHCII, except for the slight modifications from the two insertions (Tyr 76 and Glu 17) and one mutation (Phe 3). The structure reveals the location of two carbonyl carotenoids, Sx and Sn and two replaced Chl-*b* molecules. Sx and Sn are located at sites SxL2 and SnL1, corresponding to the sites L2 and L1 in plant-type LHCII, respectively, and the Chl *b* molecules are located at sites 602 and 610, which were both occupied by Chl *a* molecules in plant-type LHCII [3,4]. Both Sx and Sn bind with the *s-cis* carbonyl conformation. Sx forms two hydrogen bonds with amino acids in helix B, between the C8 carbonyl group and thiol residue of Cys 67 and between the C19 hydroxy group and peptide carbonyl of Trp 59. Sx at site SxL2 is substantially distorted from C9′ to C7′, much like lutein at the L2 site of plant LHCII [3,4]. Six nonconserved hydrophobic amino acids face Sn in the SnL1 site, while the amino acids surrounding Sx are highly conserved in the SxL2 site. Additionally, the formyl oxygen in the substituted Chl *b* at site 602 faces Sx. These results indicate that the binding pocket of Sn is highly hydrophobic, whereas that of Sx is relatively hydrophilic. In SCP, Chl *b* molecules replace two Chl *a* molecules at positions 602 and 610 in spinach LHCII. The substituted Chl *b* molecules expand the Chl *b* cluster on the stromal side into a 610-608-609-601′-602′ macrocluster.

The high-resolution, 3D structure of SCP determined in this study provides the basis for the microscopic modeling of light (energy) absorption, excitation energy transfer, and quenching in SCP, which is required to explain spectroscopic observations. Furthermore, since SCP has somewhat different pigment than plant-type LHCII with a high-resolution structure, it will provide insight into the unresolved issues regarding Chl site energies and quenching sites in plant-type LHCII.

Author contributions

SS: Conceptualization; Sample preparation; Characterization; Modeling and refining; Writing-original draft; Writing-review and editing. **TN:** Conceptualization; Methodology; Writing-review and editing. **PCH:** Cryo-EM data collection. **KS:** Cryo-EM data collection. **AK:** Cryo-EM data processing; Modeling and refining; Writing-original draft. **HT:** Modeling and refining. **PQ:** Conceptualization; Cryo-EM data collection; Cryo-EM data processing; writing-review and editing. **GK:** Conceptualization; Methodology; Writing-review and editing. **RF:** Conceptualization; Methodology; Characterization; Writing-review and

editing.

Declaration of Competing Interest

The authors declare no competing interests.

Data availability

Data will be made available on request.

Acknowledgments

RF and SS thank Ms. Tomomi Shimonaka for performing PMF analyses. RF and SS also thank Mr. Ryuichi Kano and Dr. Nami Yamano for accumulating basic knowledge about sample preparations. RF thank Prof. Tetsuro Tanabe and Prof. Nobuo Kamiya for criticism of the manuscript. The authors would like to thank Enago (www.enago.jp) for the English language review.

The grant-in-aid of the Sasakura Enviro-Science Foundation (to SS), the OCU Strategic Research Grant for Basic Researches (to RF), and the JST-CREST under grant number JPMJCR20E1 (GK) were appreciated. SS thanks the Sunbor : SUNTORY Foundation for Life Sciences Bioorganic Research Institute for a scholarship (FY2020-2023). This work was performed in part under the Collaborative Research Program of the Institute for Protein Research, Osaka University (CR-21-02 to RF), and the joint research program of the Artificial Photosynthesis, Osaka City University (FY2018 to TN).

Supplementary materials

Supplementary material associated with this article can be found, in the online version, at doi:10.1016/j.bbadva.2022.100064.

References

[1] R. Croce, H. Van Amerongen, Light harvesting in oxygenic photosynthesis: Structural biology meets spectroscopy, Science 369 (2020) eaay2058.
[2] A.V. Ruban, F. Saccon, Chlorophyll a de-excitation pathways in the LHCII antenna, J. Chem. Phys. 156 (2022), 070902, https://doi.org/10.1063/5.0073825.
[3] Z. Liu, et al., Crystal structure of spinach major light-harvesting complex at 2.72 Å resolution, Nature 428 (2004) 287–292, https://doi.org/10.1038/nature02373.
[4] J. Standfuss, A.C.T. van Scheltinga, M. Lamborghini, W. Kühlbrandt, Mechanisms of photoprotection and nonphotochemical quenching in pea light-harvesting complex at 2.5 Å resolution, EMBO J. 24 (2005) 919–928, https://doi.org/10.1038/sj.emboj.7600585.
[5] V. Novoderezhkin, A. Marin, R. Grondelle, Intra- and inter-monomeric transfers in the light harvesting LHCII complex: the Redfield–Förster picture, Phys. Chem. Chem. Phys. 13 (2011) 17093–17103, https://doi.org/10.1039/C1CP21079C.
[6] F. Müh, M.E. Madjet, T. Renger, Structure-based identification of energy sinks in plant light-harvesting complex II, J. Phys. Chem. B 114 (2010) 13517–13535, https://doi.org/10.1021/jp106323e.
[7] C. Curutchet, B. Mennucci, Quantum chemical studies of light harvesting, Chem. Rev. 117 (2017) 294–343, https://doi.org/10.1021/acs.chemrev.5b00700.
[8] T.P.J. Krüger, V.I. Novoderezhkin, E. Romero, R. van Grondelle, in: J. Golbeck, A. van der Est (Eds.), The Biophysics of Photosynthesis. Biophysics for the Life Sciences, 11, Springer, New York, NY, 2014. https://doi.org/10.1007/978-1-4939-1148-6_3.
[9] V. Sláma, L. Cupellini, B. Mennucci, Exciton properties and optical spectra of light harvesting complex II from a fully atomistic description, Phys. Chem. Chem. Phys. 22 (2020) 16783, https://doi.org/10.1039/D0CP02492A.
[10] C. Gray, T. Wei, T. Polivka, V. Daskalakis, C.D.P. Duffy, Trivial excitation energy transfer to carotenoids is an unlikely mechanism for non-photochemical quenching in LHCII, Front. Plant Sci. 12 (2022), 797373, https://doi.org/10.3389/fpls.2021.797373.
[11] D. Krause-Jensen, C Duarte, Substantial role of macroalgae in marine carbon sequestration, Nat. Geosci. 9 (2016) 737–742, https://doi.org/10.1038/ngeo2790.
[12] A.S. Chapman, From introduced species to invader: what determines variation in the success of Codium fragile ssp.tomentosoides (Chlorophyta) in the North Atlantic Ocean? Helgolander Meeresunters 52 (1998) 277–289, https://doi.org/10.1007/BF02908902.
[13] M. Stomp, J. Huisman, L.J. Stal, H.C.P Matthijs, Colorful niches of phototrophic microorganisms shaped by vibrations of the water molecule, ISME J. 1 (2007) 271–282, https://doi.org/10.1038/ismej.2007.59.
[14] J.M. Anderson, Chlorophyll-protein complexes of a Codium species, including a light-harvesting siphonaxanthin-Chlorophyll a/b-protein complex, an evolutionary relic of some Chlorophyta, Biochim. Biophys. Acta 724 (1983) 370–380, https://doi.org/10.1016/0005-2728(83)90096-8.
[15] Y. Yokohama, A. Kageyama, T. Ikawa, S. Shimura, A carotenoid characteristic of chlorophycean seaweeds living in deep coastal waters, Bot. Mar. (1977) 433–436, https://doi.org/10.1515/botm.1977.20.7.433. XX.
[16] S. Akimoto, et al., Ultrafast excitation relaxation dynamics and energy transfer in the siphonaxanthin-containing green alga Codium fragile, Chem. Phys. Lett. 390 (2004) 45–49, https://doi.org/10.1016/j.cplett.2004.03.140.
[17] W. Wang, et al., Spectral and functional studies on siphonaxanthin-type light-harvesting complex of photosystem II from Bryopsis corticulans, Photosynth. Res. 117 (2013) 267–279, https://doi.org/10.1007/s11120-013-9808-3.
[18] S. Streckaite, et al., Pigment structure in the light-harvesting protein of the siphonous green alga Codium fragile, Biochim. Biophys. Acta 1862 (2021), 148384, https://doi.org/10.1016/j.bbabio.2021.148384.
[19] G. Christa, et al., Photoprotection in a monophyletic branch of chlorophyte algae is independent of energy-dependent quenching (qE), New Phytol. 214 (2017) 1132–1144, https://doi.org/10.1111/nph.14435.
[20] C. Iha, et al., Genomic adaptations to an endolithic lifestyle in the coral-associated alga Ostreobium, Curr. Biol. 31 (7) (2021) 1393–1402, https://doi.org/10.1016/j.cub.2021.01.018.
[21] P. Akhtar, et al., Spectral tuning of light-harvesting complex II in the siphonous alga Bryopsis corticulans and its effect on energy transfer dynamics, Biochim. Biophys. Acta 1861 (7) (2020), 148191, https://doi.org/10.1016/j.bbabio.2020.148191.
[22] H.L. Nguyen, et al., An exciton dynamics model of bryopsis corticulans light-harvesting complex II, J. Phys. Chem. B 125 (2021) 1134–1143, https://doi.org/10.1021/acs.jpcb.0c10634.
[23] T.H.P. Brotosudarmo, B. Wittmann, S. Seki, R. Fujii, J. Köhler, Preprocess dependence of optical properties of ensembles and single siphonaxanthin-containing major antenna from the marine green alga Codium fragile, Sci. Rep. 12 (2022) 8461, https://doi.org/10.1038/s41598-022-11572-3.
[24] T.H.P. Brotosudarmo, B. Wittmann, S. Seki, R. Fujii, J. Köhler, Wavelength-dependent optical response of single photosynthetic antenna complexes from siphonous green alga codium fragile, J. Phys. Chem. Lett. 13 (2022) 5226–5231, https://doi.org/10.1021/acs.jpclett.2c01160.
[25] S. Seki, et al., Discovery of a novel siphonaxanthin biosynthetic precursor in Codium fragile accumulated only by blue-green exposure, FEBS Lett. 596 (2022) 1544–1555, https://doi.org/10.1002/1873-3468.14357.
[26] R. Raniello, M. Lorenti, C. Brunet, M.C. Buia, Photoacclimation of the invasive alga Caulerpa racemosa var. cylindracea to depth and daylight patterns and a putative new role for siphonaxanthin, Mar. Ecol. 27 (2006) 20–30, https://doi.org/10.1111/j.1439-0485.2006.00080.x.
[27] C. Uragami, et al., Light-dependent conformational change of neoxanthin in a siphonous green alga, *Codium intricatum*, revealed by Raman spectroscopy, Photosynth. Res. 121 (2014) 69–77, https://doi.org/10.1007/s11120-014-0011-y.
[28] K. Sader, et al., Industrial cryo-EM facility setup and management, Acta Cryst. D 76 (2020) 313–325, https://doi.org/10.1107/S2059798320002223.
[29] S.Q. Zheng, et al., MotionCor2: anisotropic correction of beam-induced motion for improved cryo-electron microscopy, Nat. Method. 14 (2017) 331–332, https://doi.org/10.1038/nmeth.4193.
[30] K. Zhang, Gctf: Real-time CTF determination and correction, J. Struct. Biol. 193 (2016) 1–12, https://doi.org/10.1016/j.jsb.2015.11.003.
[31] J. Zivanov, et al., New tools for automated high-resolution cryo-EM structure determination in RELION-3, eLife 7 (2018) e42166, https://doi.org/10.7554/eLife.42166.
[32] A. Punjani, J.L. Rubinstein, D.J. Fleet, M.A. Brubaker, CryoSPARC: algorithms for rapid unsupervised cryo-EM structure determination, Nat. Method. 14 (2017) 290–296, https://doi.org/10.1038/nmeth.4169.
[33] P. Emsley, B. Lohkamp, W. Scott, K. Cowtan, Features and development of coot, Acta Crystallogr. D Biol. Crystallogr. 66 (2010) 486–501, https://doi.org/10.1107/S0907444910007493.
[34] P.D. Adams, et al., PHENIX: a comprehensive Python-based system for macromolecular structure solution, Acta Crystallogr. D 4 (2010) 43–44, https://doi.org/10.1107/S0907444909052925.
[35] E.F. Pettersen, et al., UCSF Chimera–a visualization system for exploratory research and analysis, J Comput. Chem. 25 (2004) 1605–1612, https://doi.org/10.1002/jcc.20084.
[36] C.J. Gisriel, J. Wang, G.W. Brudvig, D.A. Bryant, Opportunities and challenges for assigning cofactors in cryo-EM density maps of chlorophyll-containing proteins, Commun. Biol. 3 (2020) 408, https://doi.org/10.1038/s42003-020-01139-1.
[37] C.J. Gisriel, et al., Quantitative assessment of chlorophyll types in cryo-EM maps of photosystem I acclimated to far-red light, Biochim. Biophys. Acta Adv. 1 (2021), 100019, https://doi.org/10.1016/j.bbadva.2021.100019.
[38] L. Nicol, R. Croce, Light harvesting in higher plants and green algae, in: R. Croce, R. van Grondelle, H. van Amerongen, I. van Stokkum (Eds.), Light Harvesting in Photosynthesis, 1st Ed., CRC Press, Boca Raton, 2018. Chapter 4.
[39] W. Wang, J.R. Shen, Structure, structure, organization and function of light-harvesting complexes associated with photosystem II, in: JR. Shen, K. Satoh, S. I. Allakhverdiev (Eds.), Photosynthesis: Molecular Approaches to Solar Energy Conversion. Advances in Photosynthesis and Respiration, Springer, Cham, 2021 vol 47.
[40] K. Zhang, G.D. Pintilie, S. Li, et al., Resolving individual atoms of protein complex by cryo-electron microscopy, Cell Res. 30 (2020) 1136–1139, https://doi.org/10.1038/s41422-020-00432-2.

[41] G. Dubertet, C. Gerard-Hirne, A. Trémolières, Importance of trans-Δ3-hexadecenoic acid containing phosphatidylglycerol in the formation of the trimeric light-harvesting complex in Chlamydomonas, Plant Physiol. Biochem. 40 (2002) 829–836, https://doi.org/10.1016/S0981-9428(02)01442-0.
[42] J. Engelken, C. Funk, I. Adamska, The extended light-harvesting complex (LHC) protein superfamily: Classification and evolutionary dynamics, in: R. Burnap, W. Vermaas (Eds.), Functional Genomics and Evolution of Photosynthetic Systems. Advances in Photosynthesis and Respiration, Springer, Dordrecht, 2012, https://doi.org/10.1007/978-94-007-1533-2_11 vol. 33.
[43] T. Polivka, V. Sundström, Ultrafast dynamics of carotenoid excited states−from solution to natural and artificial systems, Chem. Rev. 104 (2004) 2021–2072, https://doi.org/10.1021/cr020674n.
[44] H. Hashimoto, et al., Understanding/unravelling carotenoid excited singlet states, J. R. Soc. Interface 15 (2021), 20180026, https://doi.org/10.1098/rsif.2018.0026.
[45] R. Nagao, et al., Structural basis for different types of hetero-tetrameric light-harvesting complexes in a diatom PSII-FCPII supercomplex, Nat. Commun. 13 (2022), 1764, https://doi.org/10.1038/s41467-022-29294-5.
[46] Y. Yamano, M. Mimuro, M. Ito, Carotenoids and related polyenes. Part 4.1 synthesis of carotenoid analogues containing a conjugated carbonyl group and their fluorescence properties, J. Chem. Soc., Perkin Trans. 1 (1997) 2713–2724, https://doi.org/10.1039/A702815F.
[47] H. Staleva-Musto, et al., Intramolecular charge-transfer state of carotenoids siphonaxanthin and siphonein: function of non-conjugated acyl-oxy group, Photosynth. Res. 144 (2020) 127–135, https://doi.org/10.1007/s11120-019-00694-x.
[48] P. Zhou, F. Tian, F. Lv, Z. Shang, Geometric characteristics of hydrogen bonds involving sulfur atoms in proteins, Proteins 76 (2009) 151–163, https://doi.org/10.1002/prot.22327.
[49] S. Akimoto, et al., Identification of a new excited state responsible for the in vivo unique absorption band of siphonaxanthin in the green alga codium fragile, J. Phys. Chem. B 111 (2007) 9179–9181, https://doi.org/10.1021/jp071766p.
[50] S. Akimoto, et al., Solvent effects on excitation relaxation dynamics of a keto-carotenoid, siphonaxanthin, Photochem. Photobiol. Sci. 7 (2008) 1206–1209, https://doi.org/10.1039/B802658K.
[51] A.V. Ruban, A.P. Pascal, B. Robert, Xanthophylls of the major photosynthetic light-harvesting complex of plants: identification, conformation and dynamics, FEBS Lett. 477 (2000) 181–185, https://doi.org/10.1016/S0014-5793(00)01799-3.
[52] H. Yan, et al., Two lutein molecules in LHCII have different conformations and functions: insights into the molecular mechanism of thermal dissipation in plants, Biochem. Biophys. Res. Commun. 355 (2007) 457–463, https://doi.org/10.1016/j.bbrc.2007.01.172.
[53] K. Nakayama, M. Mimuro, Chlorophyll forms and excitation energy transfer pathways in light-harvesting chlorophyll a/b-protein complexes isolated from the siphonous green alga, Bryopsis maxima, Biochim. Biophys. Acta 1184 (1994) 103–110, https://doi.org/10.1016/0005-2728(94)90159-7.
[54] T.P.J. Krüger, et al., Disentangling the low-energy states of the major light-harvesting complex of plants and their role in photoprotection, Biochim. Biophys. Acta 1837 (2014) 1027–1038, https://doi.org/10.1016/j.bbabio.2014.02.014.